RSC Advances

ROYAL SOCIETY OF CHEMISTRY

www.rsc.org/advances

Table of contents entry

In situ synthesis of silver nanoparticles dispersed or wrapped by a *Cordyceps sinensis* exopolysaccharide in water and their catalytic activity

Zhaomin Zheng, Qilin Huang *, Han Guan, Shiyu Liu

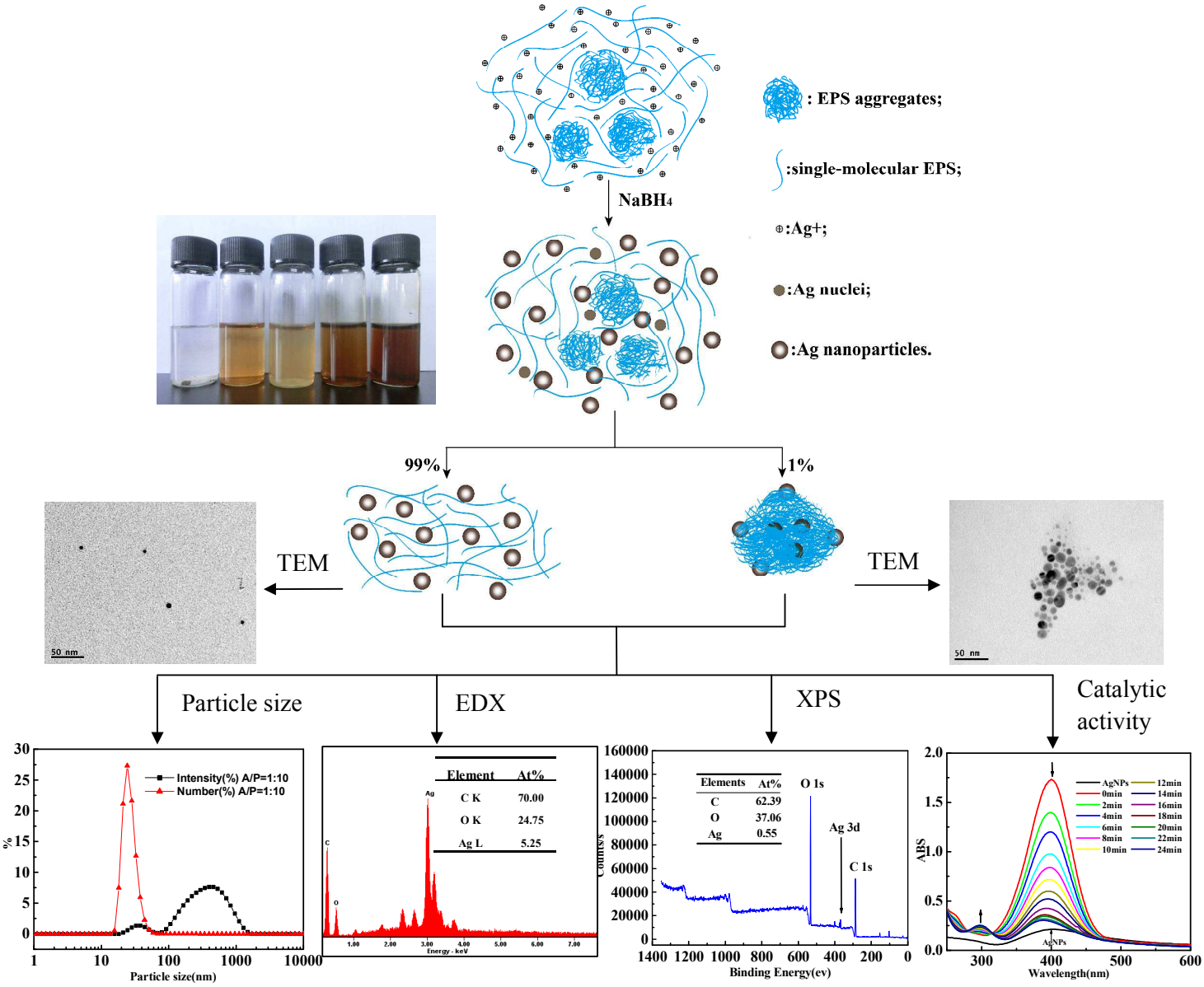

In situ synthesis of silver nanoparticles (AgNPs) dispersed or wrapped by a *Cordyceps sinensis* exopolysaccharide (EPS) and their catalytic activity.

In situ synthesis of silver nanoparticles dispersed or wrapped by a *Cordyceps sinensis* exopolysaccharide in water and their catalytic activity

Zhaomin Zheng, Qilin Huang *, Han Guan, Shiyu Liu

College of Food Science and Technology and MOE Key Laboratory of Environment Correlative Dietology, Huazhong Agricultural University, Wuhan 430070, China

* Corresponding author:

Tel: +86-15527371387; Fax: +86-027-87288375; E-mail: hql@mail.hzau.edu.cn; whuhql@gmail.com

Abstract: Well-dispersed Ag nanoparticles (AgNPs) were constructed via in situ reduction of Ag^+ under the macromolecular environment of a *Cordyceps sinensis* exopolysaccharide (EPS). The EPS-Ag nanocomposites were characterized in terms of formation, size, morphology, and Ag distribution by UV-VIS, FT-IR, laser light scattering measurements, transmission electron microscopy (TEM), energy dispersive X-ray (EDX) and X-ray photoelectron spectroscopy (XPS). Results indicated that the AgNPs in the EPS microenvironment were present in two forms: 99% of small-sized AgNPs (~5.0 nm in diameter) uniformly dispersed by single-molecular EPS and 1% of aggregated EPS-Ag nanocomposites (~300 nm in diameter). The interactions between the OH groups of the EPS and AgNPs (C-O-Ag bonds) substituted for inter- and intra-molecular interactions in native EPS, leading to good dispersion of AgNPs in the EPS matrix. Meanwhile, only a few EPS aggregates wrapped many small-sized AgNPs to form large-sized EPS-Ag nanocomposites through strong physical adsorption to O atoms of other EPS aggregates on the surfaces of AgNPs. Additionally, the introduction of dimethyl sulfoxide (DMSO) would facilitate the aggregation of AgNPs in the aqueous system. This work not only provides a simple and efficient approach to construct well-dispersed AgNPs in the aqueous system, and demonstrates the crucial role of the EPS as a biopolymer template for dispersion, stabilization and size control of AgNPs, but also finds the EPS-Ag nanocomposites can serve as a good catalyst for the reduction of 4-nitrophenol to 4-aminophenol by $NaBH_4$. The catalytic reduction had a pseudo-first-order rate constant of 1.26×10^{-3} s^{-1} and an activity parameter of 15.75 $s^{-1}g^{-1}$.

Keywords: silver nanoparticles (AgNPs); exopolysaccharide (EPS); EPS-Ag nanocomposites; *Cordyceps sinensis*; catalytic activity

1. Introduction

Recently, silver nanoparticles (AgNPs) are in the limelight as an important metal nanoparticle, because of their application in electron microscopy, optics, antimicrobials, disinfecting filters, coating materials and alkaline fuel cells.[1-3] However, AgNPs are apt to aggregate and oxidize in practical applications, indicating the necessity to improve the dispersion and stabilization of AgNPs.[4,5] In view of this, polymer-conjugated AgNPs have attracted the attention of many researchers due to their fine physiochemical properties and extensive applications.[6,7] For example, Vigneshwaran et al.[8] have reported the large-scale production of AgNPs by using soluble starch as a stabilizer, and the soluble starch-templated AgNPs can be utilized in the biomedical field. Xu et al.[9] and Singh et al.[10] synthesized the xanthan conformation-based AgNPs and the AgNPs-treated weed plant *Lantana camara's* leaf extract respectively, which exhibited favorable antimicrobial effects. Liu et al.[11] developed AgNPs-polydimethylsiloxane composite, and it offered great practical potential for the on-site monitoring and identification of pesticide residues in agricultural products and environments. Ding et al.[12] have prepared the hybrid silver-polyacrylic acid-poly (N-vinylpyrrolidone) nanogels with fluorescent and stimuli responsible properties, which have the potential application in drug delivery and biomedical imaging system.

Nowadays, polysaccharides as a class of polymers are utilized to disperse and stabilize AgNPs, including xanthan,[9] carboxymethyl cellulose,[13] chitosan[14] and sago starch,[15] etc. Additionally, bacterial exopolysaccharides from *Bacillus* are applied to encrust gold nanoparticles or stabilize iron oxide nanoparticles. [16,17] The aforementioned polysaccharides serve as an excellent template for nucleation and stabilization of nanoparticles, and thus play a crucial role in nanoscience.[7] In our previous work, an exopolysaccharide (EPS) secreted by a *Cordyceps sinensis*

fungus was isolated from mycelial fermentation medium.[18] The EPS not only had polysaccharide features of a large number of hydroxyl groups, but also exhibited quite high viscosity ([η], 2025 mL/g),[19] indicating the potential of the EPS in application as a polysaccharide template for dispersion, stabilization and size control of metal nanoparticles. Several scholars maintained that the smaller is the particle size of AgNPs, the greater will be the antimicrobial effect.[20-22] The size and distribution of AgNPs was controlled by reaction conditions such as reaction temperature,[23] time[24] and pH[1] as previously reported. In fact, the individual characteristics and the concentration of a polysaccharide will significantly influence the size of metal nanoparticles.[25] Additionally, when NaOH was introduced into the lentinan aqueous solution containing AgNPs, the AgNPs would get closer to each other, suggesting that the effect of the solvent environment on the dimension of metal nanoparticles could not be neglected.[7]

Considering the extensive use of polysaccharides as protective agents to disperse and stabilize AgNPs, it is a worthwhile endeavor to construct well-dispersed AgNPs using polysaccharide aqueous solution as matrix. In the present work, we reported the successful synthesis of well-dispersed AgNPs in the EPS aqueous solution by in situ reduction of Ag^+, and investigated the morphology and size of AgNPs as well as the Ag distribution in EPS-Ag nanocomposites by UV-VIS, FT-IR, laser light scattering measurements, transmission electron microscopy (TEM), energy dispersive X-ray (EDX) and X-ray photoelectron spectroscopy (XPS) measurements. Additionally, the effects of EPS concentration and solvent environment (dimethyl sulfoxide, DMSO) on the size and stability of AgNPs were also studied. Furthermore, the catalytic effect of the EPS-Ag nanocomposites was also investigated on the reduction of 4-nitrophenol to 4-aminophenol in the presence of $NaBH_4$. This work provides useful information regarding the

preparation of well-dispersed AgNPs using the EPS aqueous solution as matrix and the formation mechanism of EPS-Ag nanocomposites, as well as the application of AgNPs for catalytic reduction of 4-nitrophenol.

2. Experimental

2.1 Materials

The exopolysaccharide (EPS) was separated and purified by gradient ethanol precipitation from fermentation medium of a *Cordyceps sinensis* fungus Cs-HK1 as reported in our previous work.[18] All chemical reagents, i.e., $AgNO_3$ (≥99.8%), $NaBH_4$ (≥96.0%), DMSO (≥99.0%) and 4-nitrophenol (≥99.0%), were of analytical grade and purchased from Shanghai Chemical Reagent. All reagent solutions were prepared with deionized water.

2.2. Preparation of AgNPs

The AgNPs were synthesized by reducing Ag^+ directly to elemental silver (Ag^0) in the EPS aqueous solution using the reducing agent of $NaBH_4$. Briefly, different volumes (1.3-4 mL) of $AgNO_3$ solutions (1 mg/mL) were mixed with 20 mL of the EPS aqueous solution (1 mg/mL) and stirred vigorously overnight. After dropwise addition of 0.4 mL of $NaBH_4$ solution (5 mg/mL) into EPS-$AgNO_3$ mixed solutions, the colorless solutions turned yellowish-brown or brown immediately, which indicated the formation of the AgNPs. The resulting solutions were centrifuged at 8000 r/min for 20 min to remove the precipitation, and then the supernatant was filtered through a 0.45 μm pore size filter (NYL, Puradisc 13mm Syringe Filter, Whatman Inc., USA). The filtered solutions were dialyzed in a dialysis bag (Mw cutoff 14000 Da) against deionized water for 48 h. Finally, the dialyzed solutions were lyophilized to obtain the exopolysaccharide-silver nanoparticle

composites, labeled as EPS-Ag nanocomposites. The EPS-Ag nanocomposites prepared at different ratios of A/P ($AgNO_3$ to EPS) were yellowish-brown to brown flakes and stored at ambient temperature in a desiccator containing silica gel.

2.3. Characterization of the EPS-Ag nanocomposites

The ultraviolet-visible (UV-VIS) spectra of the EPS-Ag nanocomposites were performed on a UV-visible spectrophotometer (UV-1800, Shimadzu, Japan) in the range of 200-800 nm. Fourier transform-infrared (FT-IR) spectra were recorded on a FI-IR spectrometer (Nexus 470, Nicolet, UK) in the region of 400-4000 cm^{-1} using the KBr-disk method. The particle size distribution of the EPS-Ag nanocomposites at different ratios of A/P ($AgNO_3$ to EPS) was analyzed by a laser particle size analyzer (Zetasizer Nano ZS, Malvern, UK). The samples were dissolved in deionized water at a concentration of 0.1 mg/mL, and a total of fifteen runs were performed for each sample. Transmission electron microscopy (TEM) images were observed on an electron microscope (JEM2012-HT, JEOL, Japan) at an accelerating voltage of 200 kV. The EPS-Ag nanocomposites were dissolved in deionized water or the mixture of DMSO and water (7:3 by volume) at a concentration of 0.1 mg/mL, and a drop was placed on Cu grids precoated with carbon films, followed by spreading, drying at room temperature and finally observation. Energy dispersive X-ray (EDX) spectra were measured on a field emission scanning electron microscope (FESEM) (SIGMA, Carl Zeiss Company, GER) to obtain the elemental composition and distribution of the EPS-Ag nanocomposites. X-ray photoelectron spectroscopy (XPS) measurements were carried out on an X-ray photoelectron spectrometer (ESCALAB 250xi, ThermoFisher, USA) with an Al Ka X-ray source to identify the surface elemental composition and chemical state of the EPS-Ag nanocomposites.

2.4. Catalytic activity of the EPS-Ag nanocomposites

The reduction reaction of 4-nitrophenol catalyzed by the EPS-Ag nanocomposites were monitored on UV-VIS spectrophotometer (UV-1800, Shimadzu, Japan). In blank test without the EPS-Ag nanocomposites, 0.24 mL of 0.1 M $NaBH_4$ was mixed with 48 μL of 5.0 mM 4-nitrophenol in a quartz cell with a 1cm path length, leading to a color change from light yellow to yellow-green. And then the mixed solution was diluted to 3.0 mL with deionized water at final concentrations of 8 and 0.08 mM for $NaBH_4$ and 4-nitrophenol. Finally, the solution was used for UV-VIS measurement immediately. In catalytic test with the EPS-Ag nanocomposites, 48 μL of 5.0 mM 4-nitrophenol and 80 μL of 1 mg/mL EPS-Ag nanocomposites were mixed, and then 0.24 mL of 0.1 M $NaBH_4$ was added, followed by dilution to 3.0 mL. Immediately after that, the UV-VIS spectra were recorded with a time interval of 2 min at ambient temperature (25±2℃).

2.5. Data analysis

The particle size measurements were done in fifteen runs for each sample and repeated two times. Other measurements were performed in triplicate and repeated two times. The results were represented by their mean ± SD (standard deviation). The average diameter of AgNPs in several TEM images was calculated by ImageJ 1.46r software.

3. Results and discussion

3.1. Synthesis of AgNPs

During preparation, $AgNO_3$ was first well-mixed into the EPS aqueous solution, followed by the addition of $NaBH_4$ to reduce Ag^+ to Ag atoms in the EPS molecular microenvironment,

resulting in the formation of AgNPs. The process could be clearly detected by monitoring the color. Fig. 1 shows the photographs of the aqueous solutions containing AgNPs in the presence of EPS at four different A/P ratios (1:15, 1:10, 1:7 and 1:5) and the control in the absence of EPS. It can be seen that the black Ag particles were precipitated from the aqueous solution in the absence of EPS, indicating the aggregation of AgNPs due to the high surface energy of AgNPs. However, AgNPs were well dispersed in the aqueous system in the presence of EPS and exhibited a yellowish-brown to brown color with an increase in the A/P ratio. The significant difference in color of EPS-Ag aqueous solution compared with the control was derived from nanosize effects and indicated the successful synthesis of AgNPs with the yield of 0.6~1.2 g EPS-Ag / g EPS, thus demonstrating the essential role of the EPS in the formation and stabilization of AgNPs**.**

Fig. 1.

Fig. 2 shows the UV-VIS absorption spectra of the EPS-Ag nanocomposites dispersed in water at four different A/P ratios (1:15, 1:10, 1:7 and 1:5). All of the four samples exhibited similar maximum absorption peaks at ~410 nm, which corresponded well to the localized surface plasmon resonance (LSPR).[26] Based on the Mie theory,[27,28] the formed AgNPs were spherical in shape, due to the appearance of a single surface plasmon resonance (Fig. 2). This result was further confirmed by TEM. Moreover, with an increase of the A/P ratio from 1:15 to 1:10, the intensity of the maximum absorption increased gradually, indicating the increase in the concentration of AgNPs. However, the intensity of the maximum absorption decreased when the A/P ratio exceeded 1:10, suggesting the decrease in the concentration of AgNPs. The more Ag^+ was added into the system, the more Ag atoms could be produced by reduction reaction with $NaBH_4$. A large quantity of Ag atoms would be drawn together to form small clusters of Ag atoms and then generate Ag nuclei.

Finally, these Ag nuclei would grow up by aggregation to form AgNPs. The EPS with high viscosity could disperse AgNPs well to prevent AgNPs from aggregating, even precipitating, and make them stable in the aqueous solution. With the A/P ratios increased from 1:15 to 1:10, more Ag^+ existed in the system, leading to the formation of more AgNPs. The A/P ratio of 1:10 was the most suitable ratio for well dispersion of AgNPs in EPS. However, once the concentration of AgNPs exceeded the critical point (i.e., the A/P ratio exceeded 1:10), the crash between AgNPs increased rapidly, which offset the dispersive power and the protection of the EPS to AgNPs. Hence, the crash gave rise to the sticking growth between AgNPs, leading to the formation of large-sized Ag particles and precipitation from the EPS-Ag sols,[24,29] which could be demonstrated by the red shift (from 407 nm to 412 nm) and the decrease in absorption intensity of the LSPR band.[30]

Fig. 2.

The FT-IR could provide the information about the interactions between molecules.[7] Fig. 3 shows the FT-IR spectra of pure EPS and the EPS-Ag nanocomposites with different A/P values. The broad peak at 3300-3450 cm^{-1} was assigned to the stretching vibrations of O-H and a weak peak at 2924 cm^{-1} was an indication of the C-H stretching vibrations of polysaccharide.[31,32] The band at 1000-1200 cm^{-1} was attributed to the C-O antisymmetric stretching in the C-O-H and C-O-C groups of polysaccharides.[33,34] It can be clearly observed that the characteristic absorption peak of OH for the pure EPS was at 3439 cm^{-1}, while those for the EPS-Ag nanocomposites were in a higher wavenumber range (3450-3462 cm^{-1}). Additionally, the C-O-H band at 1080 cm^{-1}, which was closely related to short-range molecular interactions of polysaccharides, became weak as compared with that of pure EPS. The OH peak in the EPS-Ag nanocomposites shifted to higher

wavenumber and C-O-H band became weak, suggesting the strong interactions between the OH groups of EPS and AgNPs to disrupt hydrogen bond in native EPS and form C-O-Ag bonds.[2,25,35] During the preparation of EPS-Ag nanocomposites, the precursor Ag^+ was initially adsorbed on the chains of EPS by electrostatic interaction and then reduced in situ to Ag atoms, which destroyed the inter- and intra-molecular interactions in native EPS molecules to the formation of C-O-Ag bonds.

Fig. 3.

3.2. Size and morphology of AgNPs

As we all know, particle size can be determined with a Malvern Zetasizer Nano ZS on the principle of dynamic laser light scattering, and an equivalent sphere diameter for the particle can be derived from the Stokes-Einstein equation.[36] According to UV-VIS spectra and TEM, the AgNPs in the EPS solution were spherical, and thus the particle size of the EPS-Ag nanocomposites could be obtained from the equivalent sphere diameter measured with a Malvern Zetasizer Nano ZS. Fig. 4 shows the intensity (a) and number distribution (b) of particle sizes for the EPS-Ag nanocomposites at different A/P ratios, and the intensity distribution versus the number distribution of the EPS-Ag nanocomposites at the A/P ratio of 1:10 (c). For every A/P value (including A/P =0, i.e., pure EPS), two peaks were observed at the range of 35~90 nm and 400~500 nm in the intensity distribution profile (Fig. 4a), whereas only one peak was detected at 25~70 nm in the number distribution profile (Fig. 4b), indicating that the EPS or EPS-Ag nanocomposites were present in two different sizes and completely dominated by the small-sized particles with a percentage of 99%. With the A/P value increased from 1:15 to 1:10, the peak of small-sized particles showed a shift from large to small size (40±3 nm to 25±2 nm), but had a reverse shift (25±2 nm to 43±0.5 nm)

with the A/P value further increased to 1:5 (Figs. 4a and 4b), illustrating that the smallest size particles of 25±2 nm were formed at the A/P ratio of 1:10. Meanwhile, the intensity of large-sized particles showed a decrease, followed by a rise with the A/P value increased from 1:15 to 1:5, demonstrating the change from decrease to increase in the number of large-sized particles. These results revealed that the A/P ratio of 1:10 was beneficial to the formation of small-sized particles and the disruption of large-sized particles. With an initial increase of Ag^+, more Ag nuclei could be produced by increasing the growth rate of Ag, thus facilitating the formation of small-sized AgNPs. Conversely, when the A/P value was beyond 1:10, the formed AgNPs may aggregate together, leading to an increase in the particle size. As depicted in Fig. 4c, the large-sized particles had higher intensity than the small-sized particles, due to an enhancement of light scattering for the former. In the aqueous solution, the small-sized particles of 25±2 nm accounted for nearly 100%, suggesting the complete dominance of the small-sized particles at 25±2 nm rather than the large-sized particles.

Fig. 4.

The morphology and size of AgNPs were clearly observed by TEM. Fig. 5 shows the TEM images of the EPS-Ag nanocomposites at the A/P ratio of 1:10 in water (a and b), in 70% DMSO (c), and electron diffraction pattern of the EPS-Ag nanocomposites observed from Fig. 5b (d). As shown in Fig. 5a, the AgNPs were globular in shape, which was in line with the result from UV-VIS spectra. The average diameter of AgNPs was determined to be ~5.0 nm by counting ~750 AgNPs in many TEM images using ImageJ 1.46r software. The result was similar to the size of AgNPs synthesized from lentinan (12 nm),[7] chitosan (6.8 nm),[37] carboxymethyl chitosan (7.7 nm),[37] cellulose (8-12 nm),[38] marine macro algae polysaccharide (7-20 nm),[39] the composite films

of chitosan and sago starch (8-20 nm),[40] carboxymethyl guar grafted poly (10-20 nm)[41] and trisodium citrate (5-100 nm).[21] Moreover, it is reported that the viscosity and the molecular size of a polymer may influence the dispersion and stability of Ag particles.[42] In the present study, the AgNPs in the EPS solution had a diameter of ~5.0 nm, less than those of the aforementioned AgNPs, suggesting that the EPS could better disperse and stabilize AgNPs than other polymers due to its high viscosity. Fig. 5b shows that a large-sized particle with a diameter of ~300 nm was composed of many small-sized particles, which were proved to be AgNPs by the electron diffraction pattern in Fig. 5d. Furthermore, the small-sized AgNPs were not compactly but loosely accumulated because cavities could be observed among them. On average, only one large-sized particle was observed in every 150 AgNPs (counting ~750 AgNPs), suggesting the low proportion of large-sized particles in the EPS solution. Hence, it can be speculated that, except for a large number of single EPS molecules, there were a few EPS aggregates, which wrapped many small-sized AgNPs to form a large-sized particle (~300 nm). According to Figs. 5a and 5b, the small-sized AgNPs (~5.0 nm) were dispersed by a large number of single EPS molecules, while the large-sized EPS-Ag nanocomposites (~300 nm) were derived from the aggregation of EPS and AgNPs, which were perfectly illustrated by the emergence of two peaks in the intensity distribution of the EPS-Ag nanocomposites measured by the Malvern Zetasizer Nano ZS. Additionally, the diameter measured by TEM was smaller than that by the Malvern Zetasizer Nano ZS, which can be attributed to the fact that the Malvern Zetasizer Nano ZS measured the size of the EPS-Ag nanocomposites while TEM only observed AgNPs without EPS visualization.

To test the solvent effect, we dispersed the EPS-Ag nanocomposites in DMSO/H_2O solution and examined the morphology by TEM. It can be clearly seen that small-sized Ag particles (~5.0

nm) were hardly detected, and most of the small-sized Ag particles aggregated to form large-sized particles (even more than 600 nm in diameter) in the presence of DMSO. In the water system, the AgNPs were well-dispersed by the EPS, owing to the good solubility and high viscosity of EPS in water. In the DMSO system, the EPS could not be dissolved by DMSO, leading to the presence of EPS not as single molecules but as aggregates. Just because DMSO was a poor dispersion medium for the EPS, the AgNPs adsorbed on the EPS were not well-dispersed and stable in DMSO/H_2O solution, resulting in the aggregation, and even precipitation of AgNPs in the 70% DMSO system.

Fig. 5.

3.3. Ag distribution in the EPS-Ag nanocomposites

The elemental composition and distribution of the EPS-Ag nanocomposites could be determined by EDX, and the detected thickness is estimated to be 50~100 nm.[43,44] Fig. 6 shows the typical EDX spectra from FESEM of the EPS-Ag nanocomposites at the two A/P ratios of 1:10 (a) and 1:5 (b), together with the atomic percentage of elements. The strong Ag, C and O element peaks were observed in the EDX spectra, demonstrating the successful synthesis of the nanocomposites composed of the EPS and Ag. The strong peak appeared at ~3 keV was the typically absorption signal of Ag owing to the strong surface plasmon resonance (SPR).[45] Furthermore, the EPS-Ag nanocomposites (A/P=1:10) had a higher Ag content (5.25%) than those (A/P=1:5, 2.62%), indicating that more Ag was involved in the EPS. The result showed good coincidence with the UV-VIS data and suggested the existence of a critical value for the A/P ratio (A/P=1:10), beyond which the AgNPs would aggregate and precipitate from the sols, leading to a decrease in Ag content of the EPS-Ag nanocomposite.

Fig. 6.

As compared with EDS, the XPS could only detect the average path of 1~5 nm in solids, indicating that XPS could identify the elemental composition on the surface of the EPS-Ag nanocomposites.[46,47] Fig. 7 shows the XPS spectra at different A/P ratios (a), together with the atomic percentage of elements on the surfaces of the EPS-Ag nanocomposites, and the Ag3d spectrum of the EPS-Ag nanocomposites at the A/P ratio of 1:10 (b). As depicted in Fig. 7a, the Ag was detected on the surfaces of the EPS-Ag nanocomposites at all A/P values. The result indicated that the EPS was capped by some AgNPs, which was similar to the finding that Se nanoparticles were adsorbed on the surface of hyperbranched polysaccharide.[48] Moreover, Ag content showed an increasing trend with an elevated ratio of A/P, due to the increase in number or size of AgNPs. With the A/P ratio increased from 1:15 to 1:10, the number of AgNPs showed an increase, which was confirmed by the UV-VIS spectroscopy. However, with a further increase in the A/P ratio, the particle size rather than the number increased, which was verified by particle size analysis. The more and the larger are the AgNPs adsorbed on the surface of the EPS, the more significant will be the increase of Ag content on the surface of the EPS-Ag nanocomposites. As shown in Fig. 7b, there are two peaks at 368.2ev and 374.2ev, corresponding to the binding energies of the Ag $3d_{5/2}$ and Ag $3d_{3/2}$, respectively. The two peaks were consistent with the characteristics of metallic Ag, indicating that the AgNPs adsorbed on the EPS surface were Ag^0 particles.[49,50] This result could also elucidate that a simple adsorption of AgNPs occurred on the EPS surface. Additionally, both the AgNPs adsorbed on the EPS and the EPS capped by AgNPs might gather to form larger aggregates (Fig. 5b), so that a part of AgNPs were trapped in the EPS aggregates, which may explain why the Ag content measured by EDS was higher than that by XPS.

Fig. 7.

3.4. Schematic model of the formation of EPS-Ag nanocomposites

Based on the aforementioned results, we speculated a schematic model (Fig. 8) to depict the formation of the EPS-Ag nanocomposites. The aqueous system was filled with single-molecular and aggregated EPS, accounting for 99% and 1%, respectively (Fig. 4). Meanwhile, the precursor Ag^+ was well-dispersed by the single-molecular EPS in the aqueous system (Fig. 8a). With the dropwise addition of the reducing agent ($NaBH_4$) into the above solution, the Ag^+ was reduced in situ to Ag atoms. Thereafter, an Ag nucleus was generated by the aggregation of many small clusters of silver atoms (Fig. 8b). As the reduction proceeded, more Ag nuclei were produced, and they grew up by aggregation to form AgNPs (Fig. 8c). The speculated model could be verified by the results shown in Figs. 2-7. Moreover, as illustrated in Figs. 3, 5, 6 and 7, the interactions between AgNPs and the OH groups of EPS were very intense, leading to a good dispersion of AgNPs in the EPS molecular microenvironment. Notably, the AgNPs presented two forms in the EPS microenvironment: single-molecular EPS dispersed AgNPs with small size, and aggregated EPS-Ag nanocomposites with large size, which were derived from the existence manner of EPS in the aqueous system, i.e., the co-existence of single-molecular and aggregated EPS in the aqueous solution, accounting for 99% and 1%, respectively (Fig. 8d). The aqueous system was full of single-molecular EPS, which inhibited the further growth and aggregation of the AgNPs, resulting in the absolute dominance of the small-sized AgNPs. Additionally, the aggregated EPS-Ag nanocomposites were not neglected and generated as follows. The EPS aggregates present in the aqueous system could absorb AgNPs so that the surface of the EPS aggregates was capped by AgNPs. These EPS aggregates capped by AgNPs could gather further via the strong physical adsorption to oxygen atoms of other EPS aggregates on the surfaces of AgNPs, leading to the

formation of larger size EPS-Ag nanocomposites, which was confirmed by the results from Figs. 4-7. The overall results from this work revealed that the EPS not only acted as a matrix for the synthesis of the silver nanoparticles, but also served as a good stabilizer for AgNPs as well as the EPS-Ag nanocomposites in water.

Fig. 8.

3.5. Application of the EPS-Ag nanocomposites for catalytic reduction of 4-nitrophenol

One of potential applications of metal nanoparticles is to catalyze certain reactions that would otherwise not occur. In order to evaluate the catalytic activity of the EPS-Ag nanocomposites, the reduction of 4-nitrophenol to 4-aminophenol served as a model system.[51,52] The reduction of 4-nitrophenol to 4-aminophenol by $NaBH_4$ is kinetically restricted in the absence of a catalyst though it is thermodynamically feasible.[53] Fig. 9 shows the UV-VIS spectra of 0.08 mM 4-nitrophenol and 0.08 mM 4-nitrophenol with 8 mM $NaBH_4$ (a); 0.08 mM 4-nitrophenol with 8 mM $NaBH_4$ without any catalyst (b); 0.08 mM 4-nitrophenol with 8 mM $NaBH_4$ in the presence of EPS-Ag nanocomposites at the A/P ratio of 1:10 as catalyst (c) and plot of $\ln(A_t/A_0)$ vs. time for pseudo-first-order reduction kinetics of 4-nitrophenol by the EPS-Ag nanocomposites (d) . The color of the solution changed from light yellow to yellow-green with the addition of $NaBH_4$ to 4-nitrophenol and the absorption peak shifted from 317 to 400 nm (Fig. 9a), due to the formation of the 4-nitrophenolate ion.[51] When there were only 4-nitrophenol and $NaBH_4$ in mixed solution (in the absence of catalyst), the absorption intensity at 400 nm remained constant even after 24 min (Fig. 9b), indicating the reduction did not proceed without a catalyst. According to the aforementioned data, the EPS-Ag nanocomposites at the A/P ratio of 1:10 had the smallest particle size, implying the largest specific surface area and the highest catalytic activity, and thus this

sample was selected to explore catalytic activity. Despite the fact that AgNPs absorption is also at ~400 nm, only 80 μL of the EPS-Ag nanocomposites was used in a total volume of 3.0 mL to monitor the catalytic action and its absorbance was only 0.212 as illustrated in Fig. 9c. Thus, the overlap between the LSPR band of EPS-Ag nanocomposites and 4-nitrophenolate ion could be ignored. In the presence of the EPS-Ag nanocomposites, the absorption peak of 4-nitrophenolate ion at 400 nm gradually decreased with prolonged time. Meanwhile, a new absorption peak appeared at 298 nm, attributed to 4-aminophenol,[51] and progressively increased in intensity (Fig. 9c). This result indicated that the EPS-Ag nanocomposites could act as an effective catalyst for the reduction of 4-nitrophenol to 4-aminophenol by $NaBH_4$.

For estimating quantitatively the catalytic activity of the EPS-Ag nanocomposites, the pseudo-first-order kinetics with respect to the concentration of 4-nitrophenol was applied to calculate the rate constant (k) of this catalytic reduction reaction. Since the absorbance (A) of 4-nitrophenol is proportional to its concentration (C), the absorbance ratio A_t at time t to A_0 at $t = 0$ is equivalent to the concentration ratio C_t/C_0 of 4-nitrophenol. The kinetic equation for the catalytic reduction can be expressed as follows:

$$\ln (C_t/C_0) = \ln (A_t/A_0) = -kt$$

where C_t and C_0 are the concentration of 4-nitrophenol at time t and time $t = 0$; A_t and A_0 are the absorbance of 4-nitrophenol at time t and time $t = 0$; k is the rate constant, which can be determined from the linear plot of $\ln(A_t/A_0)$ vs. time (Fig. 9d). According to the slope of this linear plot, the rate constant was estimated to be 0.0756 min^{-1} (or 1.26×10^{-3} s^{-1}). The rate constant is not entirely appropriate to compare the catalytic efficiency of present catalyst with the ones reported in the literature with AgNP, due to different amount of the catalyst added. Therefore, the activity

parameter $\kappa = k/m$ (the ratio of rate constant k to the total mass of the catalyst added) was employed to estimate the catalytic efficiency of the catalyst.[53,54] The κ of the EPS-Ag nanocomposites was calculated to be 15.75 $s^{-1}g^{-1}$, which was much higher than the activity parameters of Fe_3O_4@SiO_2-Ag nanocomposite (7.67 $s^{-1}g^{-1}$), coral-like dendrite, banana leave-like dendrite and spherical Ag nanostructures (1.30, 0.41 and 0.09 $s^{-1}g^{-1}$).[54,55] In this work, the small-sized AgNPs (~5 nm) showed high catalytic efficiency for the reduction of 4-nitrophenol, due to having large specific surface area and more exposed Ag atoms on the surface to act as the catalytic sites. Hence, the EPS-Ag nanocomposites would serve as a good catalyst applied in homogeneous or heterogeneous catalysis.

Fig. 9.

4. Conclusions

In this work, a simple and green route to well-dispersed AgNPs was established by in situ reduction of Ag^+ in the aqueous system with the EPS as matrix. The formation, size, morphology, and the Ag distribution in the EPS-Ag nanocomposites as well as the effects of the A/P ratios and solvent were investigated. The results revealed that AgNPs existed in two forms: 99% of small AgNPs uniformly dispersed by single-molecular EPS, and 1% of aggregated EPS-Ag nanocomposites. The former presented a minimum size of ~5 nm (diameter) at the A/P ratio of 1:10, indicating good dispersion of AgNPs in water at such an EPS concentration, due to the strong interactions between the OH groups of the EPS and AgNPs (C-O-Ag bonds). The latter was derived from the EPS aggregates, which absorbed AgNPs to form the EPS aggregates capped with AgNPs and then larger size EPS-Ag nanocomposites (~300 nm in diameter) by strong physical adsorption to oxygen atoms of other EPS aggregates on the surfaces of AgNPs. In addition, the introduction of

DMSO could facilitate the aggregation of AgNPs in the aqueous system. Furthermore, the EPS-Ag nanocomposites can act as an effective catalyst for the reduction of 4-nitrophenol with high rate constant of 1.26×10^{-3} s^{-1} and activity parameter of 15.75 $s^{-1}g^{-1}$. This work not only synthesizes well-dispersed AgNPs in macromolecular environment of EPS, but also provides a good application of AgNPs for catalytic reduction of 4-nitrophenol to 4-aminophenol in the presence of $NaBH_4$.

Acknowledgements

This work was financially supported by National Natural Science Foundation of China (31401652), and Application and Foundation Research Project of Wuhan Science and Technology Bureau of China (2014020101010068).

References

1. S. M. Ghaseminezhad, S. Hamedi and S. A. Shojaosadati, *Carbohydr. Polym.,* 2012, **89**, 467-472.
2. G. R. Bardajee, Z. Hooshyar and H. Rezanezhad, *J. Inorg. Biochem.*, 2012, **117**, 367-373.
3. C.-T. Hsieh, C. Pan and W.-Y. Chen, *J. Power Sources,* 2011, **196**, 6055-6061.
4. S. Mandal, A. Gole, N. Lala, R. Gonnade, V. Ganvir and M. Sastry. *Langmuir,* 2001, **17**, 6262-6268.
5. H. S. Toh, K. Jurkschat and R. G. Compton, *Chem. Eur. J.,* 2015, **21**, 2998-3004.
6. R. A. de Matos and L. C. Courrol, *Colloids Surf. A.,* 2014, **441**, 539-543.
7. S. Li, Y. Zhang, X. Xu and L. Zhang, *Biomacromolecules,* 2011, **12**, 2864-2871.
8. N. Vigneshwaran, R. P. Nachane, R. H. Balasubramanya and P. V. Varadarajan, *Carbohydr. Res.,* 2006, **341**, 2012-2018.

9. W. Xu, W. Jin, L. Lin, C. Zhang, Z. Li, Y. Li, R. Song and B. Li, *Carbohydr. Polym.*, 2014, **101**, 961-967.
10. P. K. Singh, K. Bhardwaj, P. Dubey and A. Prabhune, *RSC Adv.*, 2015, **5**, 24513-24520.
11. S. Liu, C. Jiang, B. Yang, Z. Zhang and M. Han, *RSC Adv.*, 2014, **4**, 42358-42363.
12. Y. Ding, J. Gao, X. Yang, J. He, Z. Zhou and Y. Hu, *Adv. Powder Technol.*, 2014, **25**, 244-249.
13. V. Singh and S. Ahmad, *Cellulose,* 2012, **19**, 1759-1769.
14. S. J. Lee, D. N. Heo, J.-H. Moon, W.-K. Ko, J. B. Lee, M. S. Bae, S. W. Park, J. E. Kim, D. H. Lee, E.-C. Kim, C. H. Lee and I. K. Kwon, *Carbohydr. Polym.*, 2014, **111**, 530-537.
15. A. Mandal, S. Sekar, N. Chandrasekaran, A. Mukherjee and T. P. Sastry, *RSC Adv.*, 2015, **5**, 15763-15771.
16. G. Sathiyanarayanan, V. Vignesh, G. Saibaba, A. Vinothkanna, K. Dineshkumar, M. B. Viswanathan and J. Selvin, *RSC Adv.*, 2014, **4**, 22817-22827.
17. V. Vignesh, G. Sathiyanarayanan, G. Sathishkumar, K. Parthiban, K. Sathish-Kumar and R. Thirumurugan, *RSC Adv.*, 2015, **5**, 27794-27804.
18. Q.-L. Huang, K.-C. Siu, W.-Q. Wang, Y.-C. Cheung and J.-Y. Wu, *Process. Biochem.,* 2013, **48**, 380-386.
19. F. Sun, Q. Huang and J. Wu, *Carbohydr. Polym.*, 2014, **114**, 506-513.
20. T. Mochochoko, O. S. Oluwafemi, D. N. Jumbam and S. P. Songca, *Carbohydr. Polym.*, 2013, **98**, 290-294.
21. S. Agnihotri, S. Mukherji and S. Mukherji, *RSC Adv.*, 2014, **4**, 3974-3983.
22. J. Thiel, L. Pakstis, S. Buzby, M. Raffi, C. Ni, D. J. Pochan and S. I. Shah, *Small,* 2007, **3**, 799-803.

23. J.-K. Yan, P.-F. Cai, X.-Q. Cao, H.-L. Ma, Q. Zhang, N.-Z. Hu and Y.-Z. Zhao, *Carbohydr. Polym.*, 2013, **97**, 391-397.

24. H. Peng, A. Yang and J. Xiong, *Carbohydr. Polym.*, 2013, **91**, 348-355.

25. H. Wu, X. Li, W. Liu, T. Chen, Y. Li, W. Zheng, C. W.-Y. Man, M.-K. Wong and K.-H. Wong, *J. Mater. Chem.,* 2012, **22**, 9602-9610.

26. T. Huang and X.-H. N. Xu, *J. Mater. Chem.,* 2010, **20**, 9867-9876.

27. S. Hussain, S. A. Al-Thabaiti and Z. Khan, *Bioprocess Biosyst. Eng.,* 2014, **37**, 1727-1735.

28. D. Zhang and H. Yang, *J. Mol. Struct.,* 2014, **1060**, 1-5.

29. P. K. Rastogi, V. Ganesan and S. Krishnamoorthi, *Mat. Sci. Eng. B.*, 2012, **177**, 456-461.

30. G. P. Shevchenko, V. A. Zhuravkov, E. V. Tretyak, V. I. Shautsova and P. I. Gaiduk, *Colloids and Surfaces A: Physicochem. Eng. Aspects*, 2014, **446**, 65-70.

31. K. V. Srivatsan, N. Duraipandy, R. Lakra, S. K, U. Ramamurthy, P. S. Korrapati and M. S. Kiran, *RSC Adv.*, 2015, **5**, 22106-22116.

32. J. Wang, Z. Dong, J. Huang, J. Li, K. Liu, J. Jin and J. Ma, *RSC Adv.*, 2013, **3**, 918-922.

33. M. Kacuráková, P. Capek, V. Sasinkova, N. Wellner and A. Ebringerova, *Carbohydr. Polym.*, 2000, **43**, 195-203.

34. S. Li, Y. Shen, A. Xie, X. Yu, X. Zhang, L. Yang and C. Li, *Nanotechnology,* 2007, **18**, 405101.

35. K. I. Shingel, *Carbohydr. Res.,* 2002, **337**, 1445-1451.

36. I. Teraoka, Polymer solutions: an introduction to physical properties. A John Wiley & Sons, Inc Publication. New York, 2002.

37. M. J. Laudenslager, J. D. Schiffman and C. L. Schauer, *Biomacromolecules,* 2008, **9**, 2682-2685.

38. J. Cai, S. Kimura, M. Wada and S. Kuga, *Biomacromolecules,* 2009, **10**, 87-94.

39. H. M. El-Rafie, M. H. El-Rafie and M. K. Zahran, *Carbohydr. Polym.*, 2013, **96**, 403-410.

40. P. M. Arockianathan, S. Sekar, B. Kumaran and T. P. Sastry, *Int. J. Biol. Macromol.*, 2012, **50**, 939-946.

41. N. R. Gupta, B. L. V. Prasad, C. S. Gopinath and M. V. Badiger, *RSC Adv.*, 2014, **4**, 10261-10268.

42. A. Regiel, S. Irusta, A. Kyzioł, M. Arruebo and J. Santamaria, *Nanotechnology,* 2013, 24http://dx.doi.org/10.1088/0957-4484/24/1/015101.

43. A. J. D'Alfonso, B. Freitag, D. Klenov and L. J. Allen, *Phys. Rev. B 81,* 2010, 100101.

44. H. Golmojdeh, M. A. Zanjanchi, S. Sohrabnejad, J. Mazloom and P. Hojati-Talemi, *X-Ray Spectrom.,* 2014, **43**, 180-185.

45. P. Kanmani and S. T. Lim, *Carbohydr. Polym.*, 2013, **97**, 421-428.

46. S. M. Andersen, R. Dhiman and E. Skou, *J. Power Sources,* 2015, **274**, 1217-1223.

47. G. Yao, Y. Tang, Z. Jiang, X. An, Y. Chen and Y. Liu, *Solid State Commun.*, 2015, **201**, 98-101.

48. Y. Zhang, J. Wang and L. Zhang, *Langmuir,* 2010, **26**, 17617-17623.

49. T. C. Kaspar, T. C. Droubay and S. A. Chambers, *Thin Solid Films,* 2010, **519**, 635-640.

50. S. W. Chook, C. H. Chia, S. Zakaria, M. K. Ayob, N. M. Huang, H. M. Neoh and R. Jamal, *RSC Adv.*, 2015, **5**, 26263-26268.

51. J. Liu, G. Qin, P. Raveendran and Y. Ikushima, *Chem. Eur. J.*, 2006, **12**, 2131 – 2138.

52. A. Murugadoss and A. Chattopadhyay, *J. Phys. Chem. C,* 2008, **112**, 11265-11271.

53. B. Baruah, G. J. Gabriel, M. J. Akbashev and M. E. Booher, *Langmuir*, 2013, **29**, 4225-4234.

54. Y. Chi, Q. Yuan, Y. Li, J. Tu, L. Zhao, N. Li and X. Li, *J. Colloid Interface Sci.,* 2012, **383**, 96-102.

55. M. H. Rashid and T. K. Mandal, *J. Phys. Chem. C,* 2007, **111**, 16750-16760.

Figure Captions:

Fig. 1. Photographs of the aqueous solutions containing AgNPs in the presence of EPS at four different A/P ratios (1:15, 1:10, 1:7 and 1:5) and the control in the absence of EPS.

Fig. 2. UV-VIS absorption spectra of the EPS-Ag nanocomposites dispersed in water at four different A/P ratios (c=0.1 mg/mL).

Fig. 3. FT-IR spectra of pure EPS and the EPS-Ag nanocomposites with different A/P values.

Fig. 4. The intensity (a) and number distribution (b) of particle sizes for the EPS-Ag nanocomposites at different A/P ratios, and the intensity distribution versus the number distribution for the EPS-Ag nanocomposites at the A/P ratio of 1:10 (c).

Fig. 5. TEM images of the EPS-Ag nanocomposites at the A/P ratio of 1:10 in water (a and b), in 70% DMSO (c), and electron diffraction pattern of the EPS-Ag nanocomposites observed from Fig. b (d) (c=0.1 mg/mL).

Fig. 6. Typical EDX spectra from FESEM of the EPS-Ag nanocomposites at the two A/P ratios of 1:10 (a) and 1:5 (b), together with the atomic percentage of elements.

Fig. 7. XPS spectra at different A/P ratios (a), together with the atomic percentage of elements on the surfaces of the EPS-Ag nanocomposites, and the Ag3d spectrum of the EPS-Ag nanocomposites at the A/P ratio of 1:10 (b).

Fig. 8. Schematic diagram of the formation process of the EPS-Ag nanocomposites.

Fig. 9. UV-VIS spectra of 0.08 mM 4-nitrophenol and 0.08 mM 4-nitrophenol with 8 mM $NaBH_4$ (a); 0.08 mM 4-nitrophenol with 8 mM $NaBH_4$ without any catalyst (b); 0.08 mM 4-nitrophenol with 8 mM $NaBH_4$ in the presence of EPS-Ag nanocomposites at the A/P ratio of 1:10 as catalyst (c) and plot of $\ln(A_t/A_0)$ vs. time for pseudo-first-order reduction kinetics of 4-nitrophenol by the

EPS-Ag nanocomposites (d).

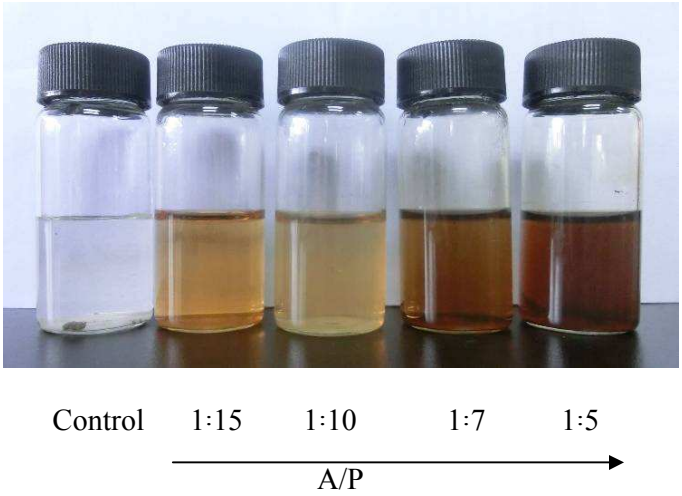

Fig. 1. Photographs of the aqueous solutions containing AgNPs in the presence of EPS at four different A/P ratios (1:15, 1:10, 1:7 and 1:5) and the control in the absence of EPS.

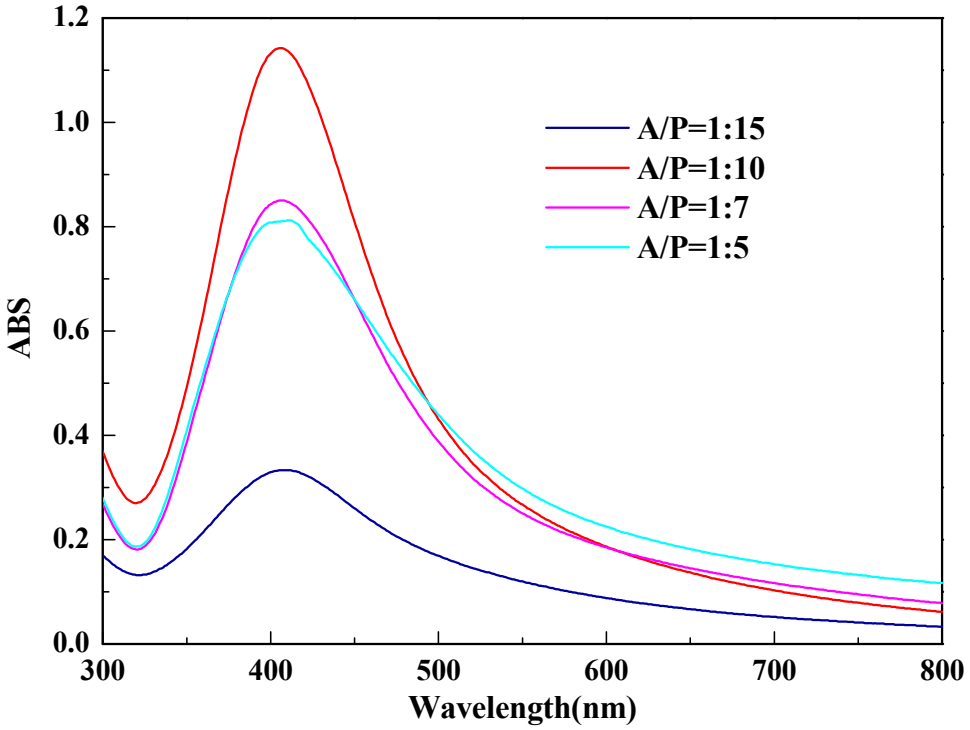

Fig. 2. UV-VIS absorption spectra of the EPS-Ag nanocomposites dispersed in water at four different A/P ratios (*c*=0.1 mg/mL).

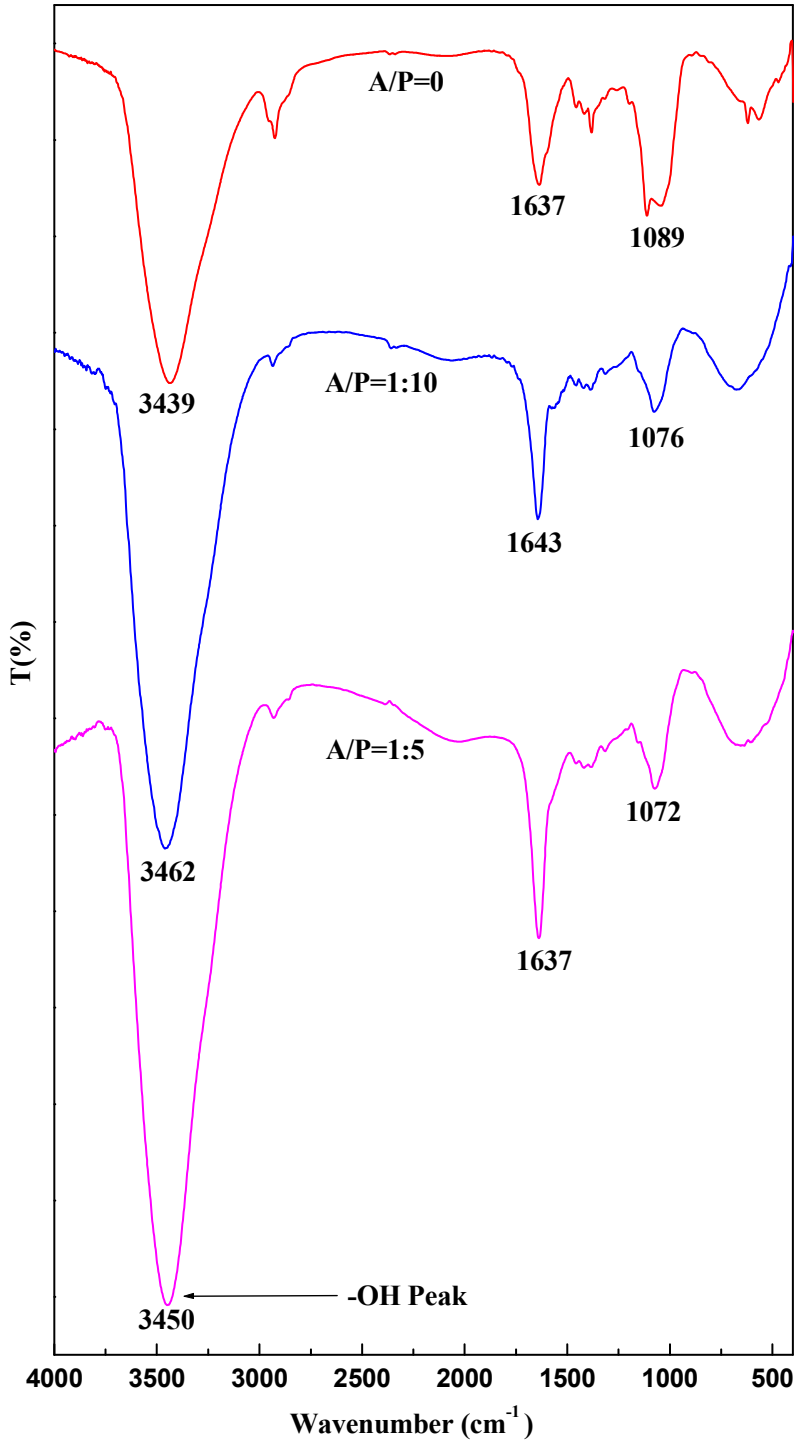

Fig. 3. FT-IR spectra of pure EPS and the EPS-Ag nanocomposites with different A/P values.

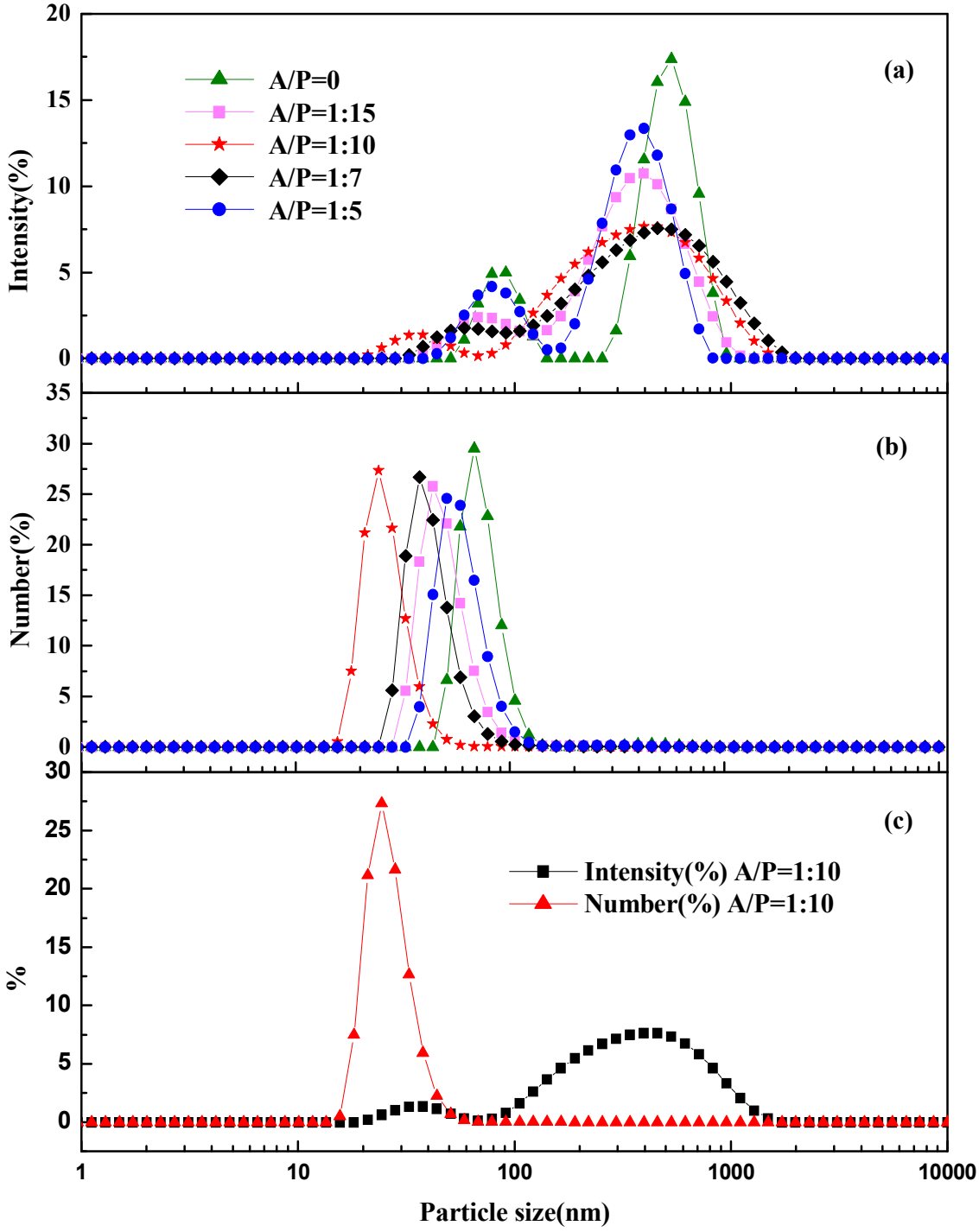

Fig. 4. The intensity (a) and number distribution (b) of particle sizes for the EPS-Ag nanocomposites at different A/P ratios, and the intensity distribution versus the number distribution for the EPS-Ag nanocomposites at the A/P ratio of 1:10 (c).

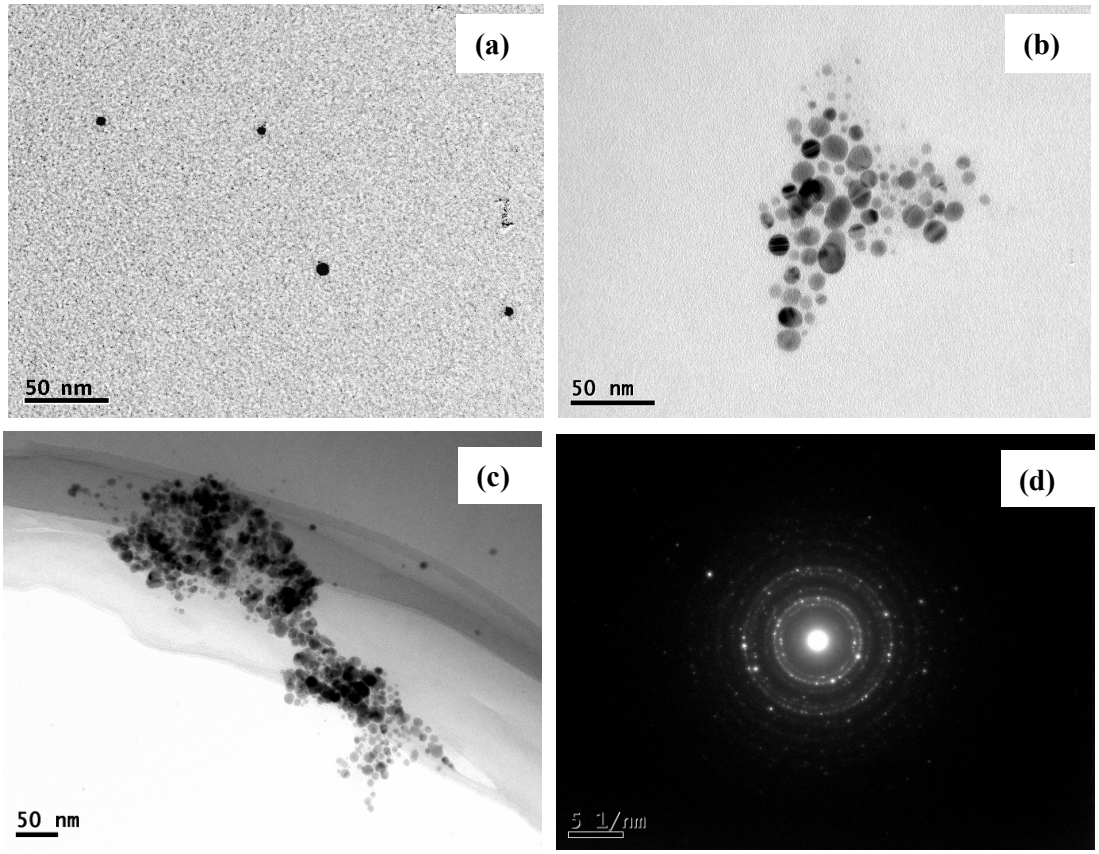

Fig. 5. TEM images of the EPS-Ag nanocomposites at the A/P ratio of 1:10 in water (a and b), in 70% DMSO (c), and electron diffraction pattern of the EPS-Ag nanocomposites observed from Fig. b (d) (*c*=0.1 mg/mL).

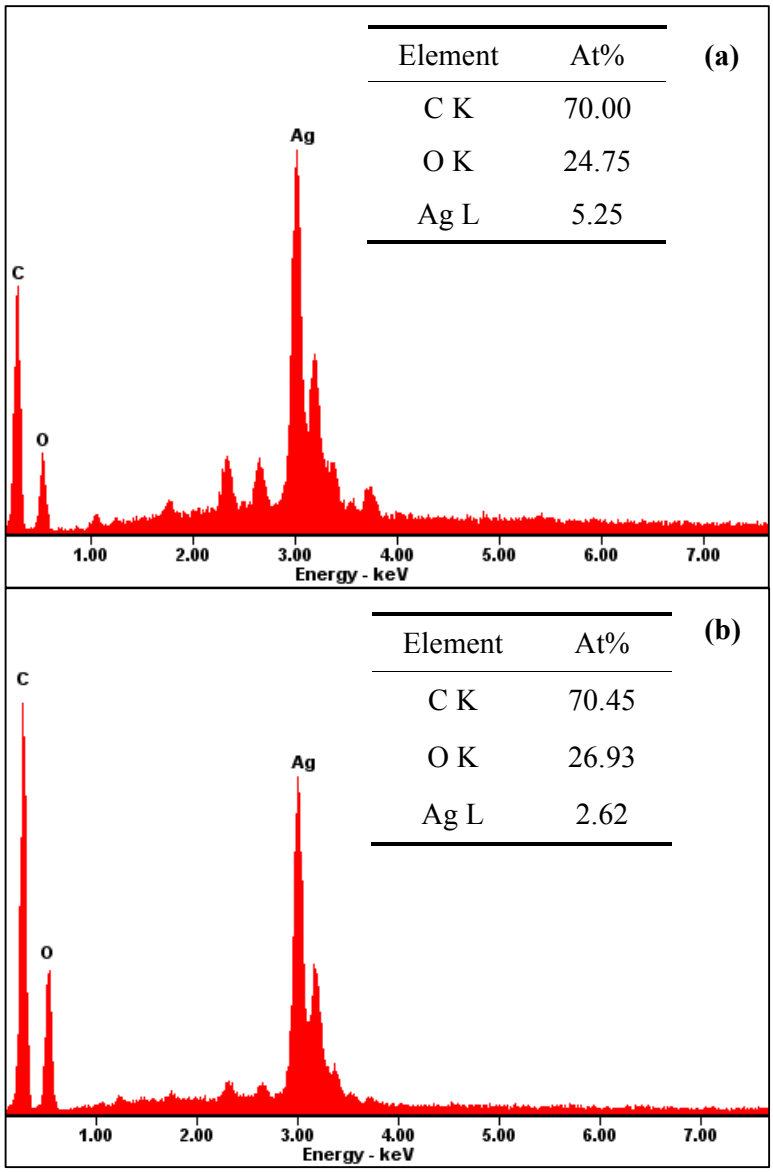

Fig. 6. Typical EDX spectra from FESEM of the EPS-Ag nanocomposites at the two A/P ratios of 1:10 (a) and 1:5 (b), together with the atomic percentage of elements.

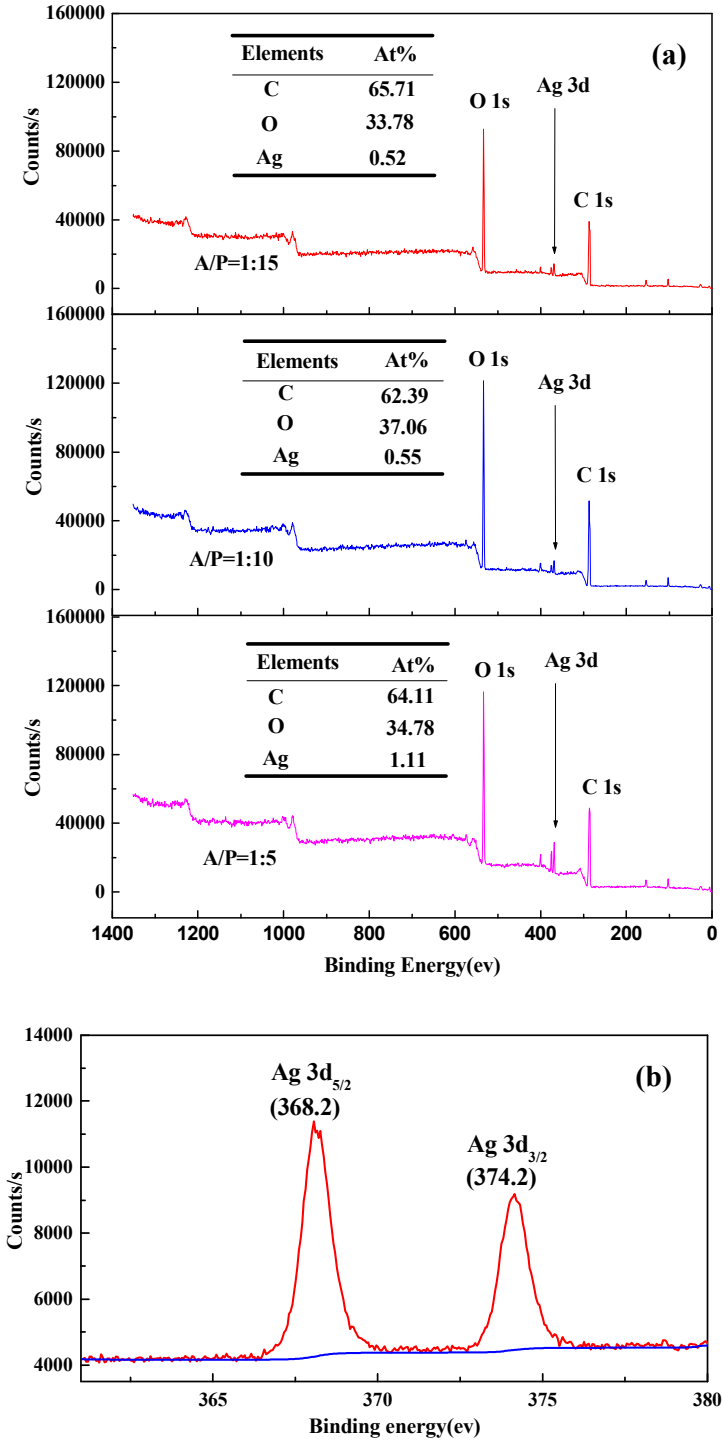

Fig. 7. XPS spectra at different A/P ratios (a), together with the atomic percentage of elements on the surfaces of the EPS-Ag nanocomposites, and the Ag3d spectrum of the EPS-Ag nanocomposites at the A/P ratio of 1:10 (b).

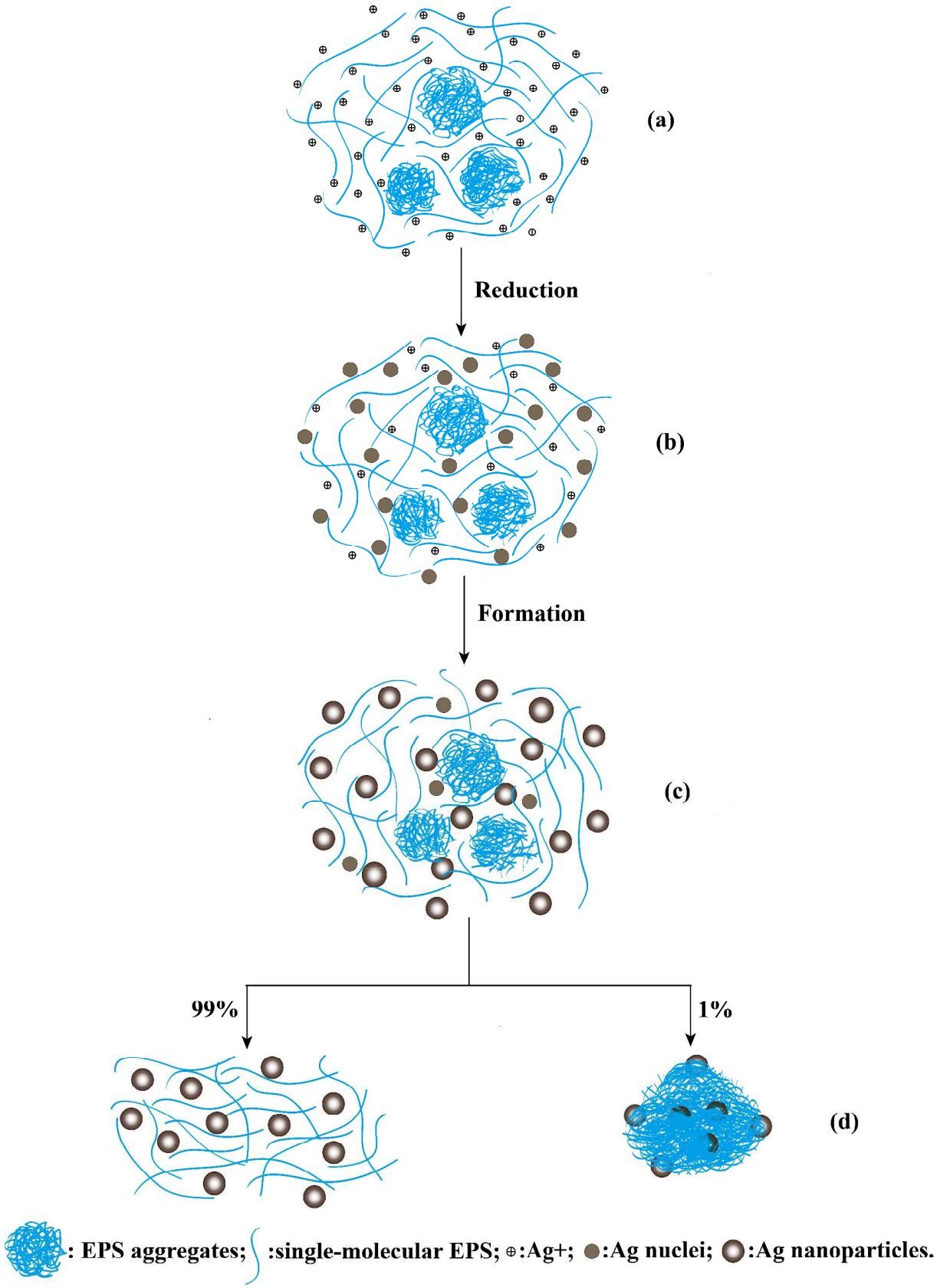

Fig. 8. Schematic diagram of the formation process of the EPS-Ag nanocomposites.

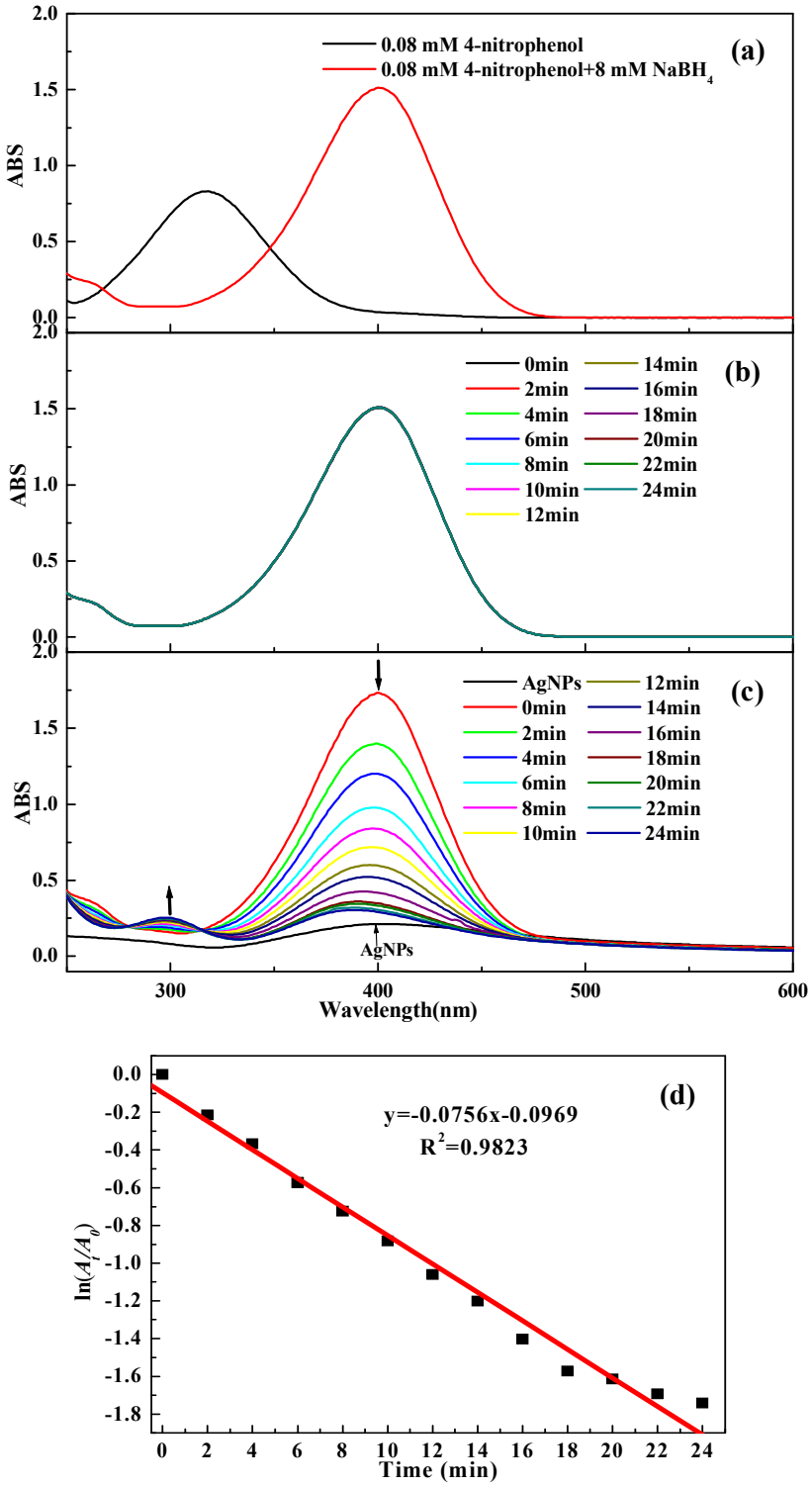

Fig. 9. UV-VIS spectra of 0.08 mM 4-nitrophenol and 0.08 mM 4-nitrophenol with 8 mM $NaBH_4$ (a); 0.08 mM 4-nitrophenol with 8 mM $NaBH_4$ without any catalyst (b); 0.08 mM 4-nitrophenol with 8 mM $NaBH_4$ in the presence of EPS-Ag nanocomposites at the A/P ratio of 1:10 as catalyst (c) and plot of $\ln(A_t/A_0)$ vs. time for pseudo-first-order reduction kinetics of 4-nitrophenol by the EPS-Ag nanocomposites (d).